ResearchGate

See discussions, stats, and author profiles for this publication at: https://www.researchgate.net/publication/229158928

Reversibility of Prion Misfolding: Insights from Constant-pH Molecular Dynamics Simulations

ARTICLE *in* THE JOURNAL OF PHYSICAL CHEMISTRY B · JULY 2012

Impact Factor: 3.3 · DOI: 10.1021/jp3034837 · Source: PubMed

CITATIONS
18

READS
20

4 AUTHORS:

Diogo Vila-Vicosa
University of Lisbon
17 PUBLICATIONS **72** CITATIONS
SEE PROFILE

Sara R. R. Campos
New University of Lisbon
13 PUBLICATIONS **122** CITATIONS
SEE PROFILE

Antonio Baptista
New University of Lisbon
91 PUBLICATIONS **2,026** CITATIONS
SEE PROFILE

Miguel Machuqueiro
University of Lisbon
36 PUBLICATIONS **704** CITATIONS
SEE PROFILE

Available from: Miguel Machuqueiro
Retrieved on: 26 January 2016

THE JOURNAL OF PHYSICAL CHEMISTRY B

Article

pubs.acs.org/JPCB

Reversibility of Prion Misfolding: Insights from Constant-pH Molecular Dynamics Simulations

Diogo Vila-Viçosa,[†] Sara R. R. Campos,[‡] António M. Baptista,[‡] and Miguel Machuqueiro*[,†]

[†]Centro de Química e Bioquímica e Departamento de Química e Bioquímica, Faculdade de Ciências, Universidade de Lisboa, 1749-016 Lisboa, Portugal

[‡]Instituto de Tecnologia Química e Biológica, Universidade Nova de Lisboa, Av. da República, EAN, 2780-157 Oeiras, Portugal

Supporting Information

ABSTRACT: The prion protein (PrP) is the cause of a group of diseases known as transmissible spongiform encephalopathies (TSEs). Creutzfeldt−Jakob disease and bovine spongiform encephalopathy are examples of TSEs. Although the normal form of PrP (PrP^C) is monomeric and soluble, it can misfold into a pathogenic form (PrP^{Sc}) that has a high content of β-structure and can aggregate forming amyloid fibrils. The mechanism of conversion of PrP^C into PrP^{Sc} is not known but different triggers have been proposed. It can be catalyzed by a PrP^{Sc} sample, or it can be induced by an external factor, such as low pH. The pH effect on the structure of PrP was recently studied by computational methods [Campos et al. *J. Phys. Chem. B* **2010**, *114*, 12692−12700], and an evident trend of loss of helical structure was observed with pH decrease, together with a gain of β-structures. In particular, one simulation at pH 2 showed an evident misfolding transition. The main goal of the present work was to study the effects of a change in pH to 7 in several transient conformations of this simulation, in order to draw some conclusions about the reversibility of PrP misfolding. Although the most significant effect caused by the change of pH to 7 was a global stabilization of the protein structure, we could also observe that some conformational transitions induced by pH 2 were reversible in many of our simulations, namely those started from the early moments of the misfolding transition. This observation is in good agreement with experiments showing that, even at pH as low as 1.7, it is possible to revert the misfolding process [Bjorndahl et al. *Biochemistry* **2011**, *50*, 1162−1173].

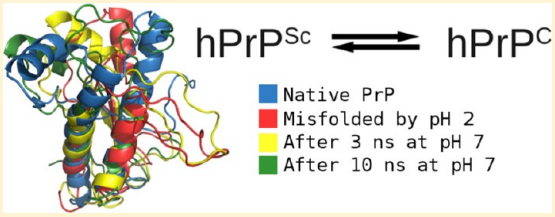

INTRODUCTION

The cellular form of the prion protein (PrP^C) is a glycosylated, glycosylphosphatidylinositol-anchored component of the outer surface of neuron cells and appears to have an important role in the signal transduction pathway involving Cu^{2+}.[1,2] There are several structures of human PrP (huPrP) in the Protein Data Bank.[3−5] According to these data, the huPrP contains a N-terminus (Nter) region with no defined structure (amino acids (aa) 23−124) and a globular core (aa 125−228) composed of three α-helices (HA: aa 144−156; HB: aa 174−194; HC: aa 200−228) and a small β-sheet (aa 128−131 + aa 161−164). It has a disulfide bond between C179 and C214 and two N-glycosylation sites (N181 and N197). The Nter region is characterized by octarepeats (aa 51−91) that appear to acquire a structure in the presence of Cu^{2+} or other metals.[2,6]

Although there are many processes in which PrP appears to have an important role, its function remains unknown.[7] However, it is known to play a crucial role in a class of diseases known as transmissible spongiform encephalopathies (TSEs).[8−16] TSEs are a class of neurodegenerative diseases, which are fatal and for which there is no known treatment yet. Scrapie in sheep, bovine spongiform encephalopathy in cattle, and Creutzfeldt−Jakob disease, Gerstmann−Sträussler−Scheinker syndrome, kuru, and fatal familial insomnia in humans are examples of TSEs. The biochemical features associated with TSEs are the accumulation of amyloid deposits, vacuolation, and astroglial proliferation in the brain.

Prusiner proposed that the scrapie disease was caused by a proteinaceous infectious particle he had identified and that nowadays is known as the "scrapie" form of PrP (PrP^{Sc}).[17] Although PrP^C and PrP^{Sc} are chemically equivalent, it has been shown that there are large structural differences between them, specifically in terms of secondary structure.[18] While PrP^C has a high α-helix content (∼42%) and a low content in β-sheet (∼3%), PrP^{Sc} acquires a high content in β-sheet (∼43%) and its α-helix content decreases to ∼30%.[18] Moreover, while PrP^C is monomeric, soluble, and protease K sensitive, PrP^{Sc} may aggregate forming insoluble and protease K resistant amyloid fibrils.[9,13,16] According to the protein-only hypothesis, PrP^{Sc} can act as a template in the misfolding of PrP^C, and it is the only infectious agent.[12,16] Despite the misfolding mechanism of the spontaneous conversion of PrP^C into PrP^{Sc} not being completely clarified, it has been observed that PrP^C cycles between the cell surface and the endocytic pathway,[19,20] and it has been proposed that the conversion between PrP^C and PrP^{Sc} can be induced by the low pH present in late endosomes.[21−28] Nevertheless the NMR structures at pH 7.0[3] and pH 4.5[4] have

Received: April 11, 2012
Revised: June 21, 2012
Published: June 26, 2012

ACS Publications © 2012 American Chemical Society

dx.doi.org/10.1021/jp3034837 | *J. Phys. Chem. B* 2012, 116, 8812−8821

the same global fold with only slight differences, which reflects the fact that PrP^C is metastable at pH 4.5, taking about a week to convert into PrP^{Sc}.[28]

It is not known if the conversion of PrP^C into PrP^{Sc} is reversible; however, it was shown that, once the disulfide bond is reduced, it is possible to observe this reversibility by circular dichroism.[25] Gerber et al. in 2008 also tried to observe this reversibility but were not successful because the global structural scaffold of PrP was irreversibly lost at low pH (in the presence of urea).[27] Interestingly, it was shown that it is possible to revert the unfolding of PrP induced by high concentrations of guanidine hydrochloride.[29] Recently, Bjorndahl et al.[30] showed that it is possible to revert the misfolding transition induced by the change in pH in the Syrian hamster PrP . In this work, the authors were able to revert the transition when it was induced by a pH value as low as 1.7. However, when the transition was induced by a pH value of 1.0, it was not possible to revert it.

As mentioned above, there are several studies related with the misfolding of PrP . However, the molecular detail of the structural transition leading to the PrP^{Sc} form remains unknown. Also, the molecular structure of this misfolded protein has not been unraveled yet, mainly because this form easily aggregates and precipitates, which hinders dramatically the use of NMR and X-ray diffraction.[31] Taking into consideration these limitations, computational methods can be very useful to elucidate the details of this conformational transition.

The structural detail of misfolding and aggregation of PrP has been studied in the past years by molecular dynamics (MD) simulations, and several triggers have been tested. High temperatures seem to induce a significant loss in secondary structure.[32−34] It has been also shown that disease associated mutations can induce several significant conformational changes,[32,33,35,36] in particular, the elongation of the native β-sheet.[35] The low pH has been studied as a factor that can induce the misfolding transition of PrP.[34,37−42] The protonation of histidine and acidic residues can also induce a movement of helix A (HA) and the loss of native contacts between this helix and the rest of the globular domain.[40] In addition, this helix seems to have a crucial role in prion aggregation.[43]

Recently, this transition was studied[42] by a constant-pH MD method[44−48] which can treat explicitly the pH as an external parameter instead of simulating a pure protonation state. Several simulations were performed at neutral and several low pH values. It was observed that a gradual acidification led to a clear trend of decrease of the average α-helix content together with the increase of the average β-sheet structure, in agreement with experimental studies.[24,26] The formation of new β-structure was observed in several simulations at pH 2 and 4, but only one replicate at pH 2 exhibited a stable β-rich structure, typical of the misfolded state. On most of the simulations at higher pH values (6 and 7), the three original helices remained very stable.

In this work, we studied the effect of reverting the pH from 2 to 7 on a set of conformations from the referred simulation at pH 2 from previous work.[42] The main goal was to answer the question of whether this conformational transition induced by low pH could be reverted by increasing the pH back to 7. In order to find some evidence of a reversibility transition, we used several conformational properties but only managed to get a clear picture when looking at the global structure of PrP.

METHODS

Simulations Setup. As indicated in the Introduction, the present reversibility study builds on our previous constant-pH MD study of PrP,[42] performed with the construct built from the NMR structure of huPrP obtained at pH 7 (1HJM,[4] segment 125−228) combined with the segment 90−123 from the NMR structure belonging to the Syrian hamster (2PRP[49]). The sets of equilibrium simulations then performed at pH 2 and 7 will be hereafter designated as Eq2 and Eq7, respectively, each consisting of a set of 12 simulations. The simulation in the set Eq2 that exhibited a stable β-rich structure, originally 40 ns long, was here extended up to 60 ns and will be designated as Eq2*; the corresponding simulation in Eq7 started with the same set of initial structure and conditions will be designated as Eq7*.

In the present work, a total number of 51 simulations at pH 7 were performed. The simulations were started from different points of the previous simulation Eq2* (see starting structures in Supporting Information, Figure S1 and S2), thus corresponding to a jump in pH. We performed 39 short jump simulations (JpS simulations) of 10 ns starting from different times (0.5, 1.0, 1.5, 2.0, 3.0, 5.0, 8.0, 11.0, 14.0, 17.0, 21.0, 25.0, and 29.0 ns) with three different replicates per each starting point (denoted, for example, as 0.5a, 0.5b, 0.5c). Also, 12 long jump simulations (JpL simulations) of 40 ns were performed starting from 11.0, 21.0, 29.0, 30.0, 40.0, 41.2, 42.0, 47.5, 49.0, 54.5, 55.7, and 60.0 ns. All the previous and present simulations are summarized in Table 1.

Table 1. Summary of the Simulations Used in This Work

name	no. of simulations	pH	duration/ns	starting point in Eq2* simulation/ns
Eq2[a]	12	2	40	
Eq2*[a]	1	2	60	
Eq7[a]	12	7	30	
Eq7*[a]	1	7	30	
JpS[b]	39[c]	7	10	0.5, 1.0, 1.5, 2.0 3.0, 5.0, 8.0, 11.0 14.0, 17.0, 21.0, 25.0, and 29.0
JpL[b]	12[d]	7	40	11.0, 21.0, 29.0, 30.0 40.0, 41.2, 42.0, 47.5, 49.0, 54.5, 55.7, and 60.0

[a]Simulations from ref 42. [b]Simulations performed in the present work. [c]Three replicates per starting point. [d]One simulation per starting point.

Constant-pH MD Settings. All simulations were performed using the stochastic titration constant-pH MD method implemented for the GROMACS package, developed by Baptista et al.[42,44−48,50] The stochastic titration method consists essentially of a MM/MD simulation in which the protonation states of the protein are periodically replaced with new states sampled by Monte Carlo (MC) using Poisson−Boltzmann (PB) derived free energy terms.

Following the methodology from the previous work,[42] in our simulations, all six His residues were titrated and acidic residues were maintained deprotonated (negatively charged); in simulation Eq2*, previously performed at pH 2 and here used as a starting point, histidines were fully protonated and acidic residues allowed to titrate. Each constant-pH MD cycle was 2 ps long and the solvent relaxation step was 0.2 ps long.

MM/MD Settings. The MM/MD simulations were performed using GROMACS 3.2.1[51−53] and the GROMOS96 53A6 force field.[54] The leapfrog algorithm was used with a 2 fs

dx.doi.org/10.1021/jp3034837 | J. Phys. Chem. B 2012, 116, 8812−8821

time step. The structures were surrounded by 16089 SPC[55] water molecules in a rhombic dodecahedral box with periodic boundary conditions. The nonbonded interactions were treated using a twin-range cutoff of 8/14 Å and updating the neighbor lists every 10 fs. Electrostatic long-range interactions were treated with a generalized reaction field[56] with a relative dielectric constant of 54[57] and an ionic strength of 0.15 M.[45] The Berendsen coupling[58] was used to treat temperature (310 K) and pressure (1 bar) with coupling constants of 0.1 and 0.5, respectively. Solvent and solute were separately coupled to the temperature bath. Isothermal compressibility of 4.5×10^{-5} bar^{-1} was used. All bonds were constrained using the LINCS algorithm.[59]

The minimization procedure used a combination of steepest descent and l-BFGS methods. The initiation was performed in 5 steps of 50 ps each with different restraints, to avoid drastic conformational changes induced by a sudden pH change.

PB/MC Settings. The PB/MC calculations were done as previously described.[60] The MEAD 2.2.0[61] software package was used for PB calculations. The atomic charges and radii[60] were taken from the GROMOS96 53A6 force field. A dielectric constant of 2 for the protein and 80 for the solvent were used. Grid spacings of 0.25, 1.0, and 2.0 Å were used in the finite difference focusing procedure.[62] The molecular surface was determined using a rolling probe of 1.4 Å and the Stern layer was 2 Å. The temperature was 310 K, and the ionic strength was 0.15 M.

The MC calculations were performed using the PETIT (version 1.5)[63] software with 10^5 steps for each calculation. Each step consisted of a cycle of random choices of protonation state (including tautomeric forms) for all individual sites and for pairs of sites with a coupling above 2.0 pK_a units,[63,64] followed by the acceptance/rejection step according to Metropolis criterion.[65]

PCA. Principal component analysis (PCA) is a method that transforms a set of variables by rotation of the axes, thus obtaining a new set of uncorrelated variables called principal components (PCs), which are ordered by their variance.[66] The selection of the first two PCs allows us to reduce the dimensionality of the data set without losing a significant amount of information. Here, we use the first two PCs to represent the conformations in only two dimensions following a previously published approach.[50]

PCA was performed using the equilibrated parts (last 20 ns) of the JpL, Eq2, and Eq7 simulations. The coordinates of the Cα of the globular core (125−228) were used. The positions were fitted to the central structure, defined as the structure that minimizes the average root-mean-square deviation after optimal rotation:[50]

$$D_i^2 = \frac{1}{n-1}\sum_{j=1}^{n} \mathrm{rmsd}_{ij}^{\,2}$$

where rmsd_{ij} is the Cα RMSD between structures i and j. This structure should be a representative one from an ensemble of conformations. The 2D space thus obtained was used to project the data and calculate energy landscapes. In this way, a kernel estimate of the data probability density[67] was computed on a grid of $(0.1\ \text{Å})^2$ bins, using a Gaussian kernel. The probability density surface was then converted to an energy surface according to

$$E(\vec{x}) = -RT \ln \frac{P(\vec{x})}{P_{\max}}$$

where $\vec{x}$ is the coordinate in the 2D space of the first two PCs and $P_{\max}$ is the maximum of the probability density function, $P(\vec{x})$.

Analyses. In the case of the long simulations Eq7, Eq2, and JpL, the equilibrated last 20 ns of each simulation were used for analysis. In the case of the short simulations JpS, the whole simulation was used. Several tools from the GROMACS software package[51−53] were used and others were developed in-house.

The DSSP criterion[68] was used to assign the secondary structure. The PyMOL 0.99 software was used to obtain rendered conformation images.

RESULTS AND DISCUSSION

Effect of the pH Jump in the Secondary Structure. We started our work by performing several long simulations corresponding to a jump from pH 2 to pH 7 (JpL) and analyzing their secondary structure evolution. The JpL simulations start mainly from later conformations of the Eq2* simulation. A high content in β structures was observed in the JpL simulations (data not shown), suggesting that these structures are also stable at pH 7, rendering the helix recovery much more difficult. In addition, we should take into consideration that the time needed for α-helix formation is experimentally estimated to be in the range from 100 ns to 1 μs,[69] thus reaching time scales completely inaccessible in this work.

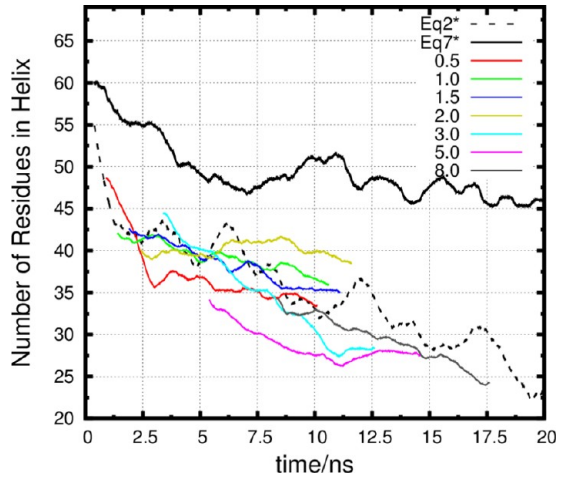

Figure 1. Variation of helix content in the JpS simulations compared with the equilibrium ones, Eq2* and Eq7*. For JpS simulations, the initial time is shifted to the Eq2* time of the conformation from which they started. Each value corresponds to the average of three replicates.

We also performed several short simulations corresponding to a jump from pH 2 to pH 7 (JpS), which started from earlier instants of the Eq2* simulation. Figure 1 represents the variation of the total number of residues in helix for the JpS simulations (started from 0.5 to 8.0 ns of the Eq2* simulation) and also for the Eq2* and Eq7* simulations. Through the comparison of the helix content in the JpS simulations with the reference curves it is possible to evaluate the initial trend of the helix content after a jump in pH from 2 to 7. There are replicates with all three possible behaviors: the helix content

dx.doi.org/10.1021/jp3034837 | J. Phys. Chem. B 2012, 116, 8812−8821

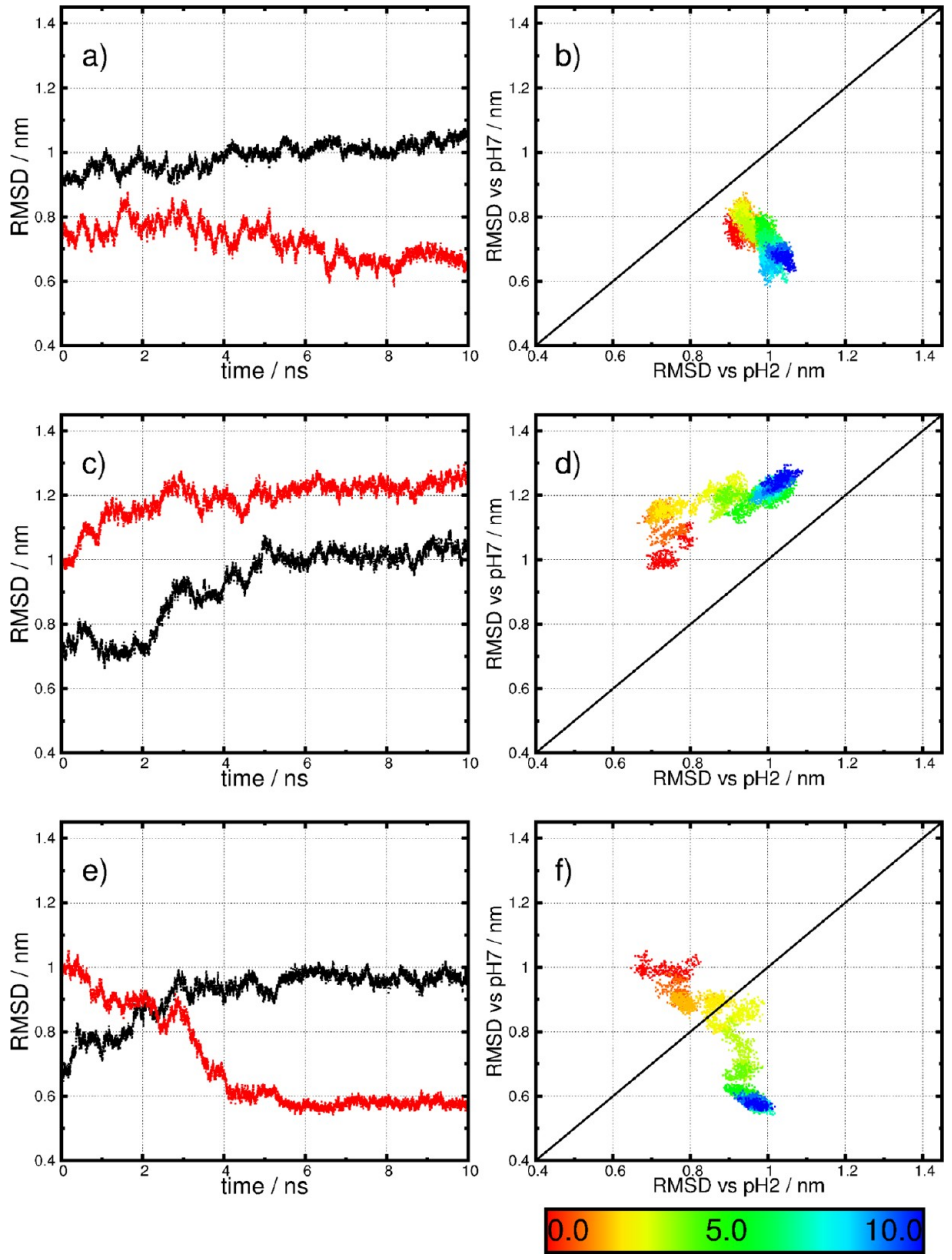

Figure 2. Left: RMSD vs central structure of Eq7 simulations (red) and RMSD vs central structure of Eq2 simulations (black). Right: scatter plots of crossed RMSD values and $x = y$ line, with the time color code in ns at the bottom. Simulations 1.5a (a, b), 8.0b (c, d), and 8.0a (e, f).

increases, decreases, or stabilizes. Nevertheless, Figure 1 shows that the global trend of the helix content is to decrease, similarly to what happens in the Eq2* simulation, even after the change to pH 7. All the replicates that are not represented in the figure follow the same trend as the Eq2* simulation (data not shown). However, after 10 ns of simulation at pH 7, the average helix content of the simulations started at t = 1.0, 1.5, and 2.0 ns is higher than in the Eq2* one. This observation indicates that pH 7 may have a slight stabilizing effect on helical structures, when compared with pH 2.

Overall, the secondary structure analysis of our simulations does not seem to indicate any kind of reversibility in the misfolding transition of PrP . Several factors can contribute to the considerable lowering in the helix content of our simulations according to the DSSP criterion. The abrupt change in pH, and the consequent addition of several new negative charges, can lead to sudden unfavorable interactions that can disrupt the global shape of a helix; although we used a smooth minimization/initiation protocol in our simulations (see Methods), it is impossible to completely avoid such instabilities. Furthermore, even if some global fold reversibility is being achieved, it may be easily missed by the strict DSSP criterion for canonical helices, whose formation can be orders of magnitude slower than our simulation times.[69] Indeed, as shown below, several simulations exhibit a behavior indicative of pH-induced reversibility.

RMSD against Central Structures of the Reference Simulations. We performed RMSD calculations for all JpS simulations to evaluate the initial trend after the change in pH (Figure 2 and Supporting Information, Figure S3). For this analysis, we chose two reference structures, namely the central structures (see Methods) from the simulations Eq2 and Eq7

dx.doi.org/10.1021/jp3034837 | J. Phys. Chem. B 2012, 116, 8812−8821

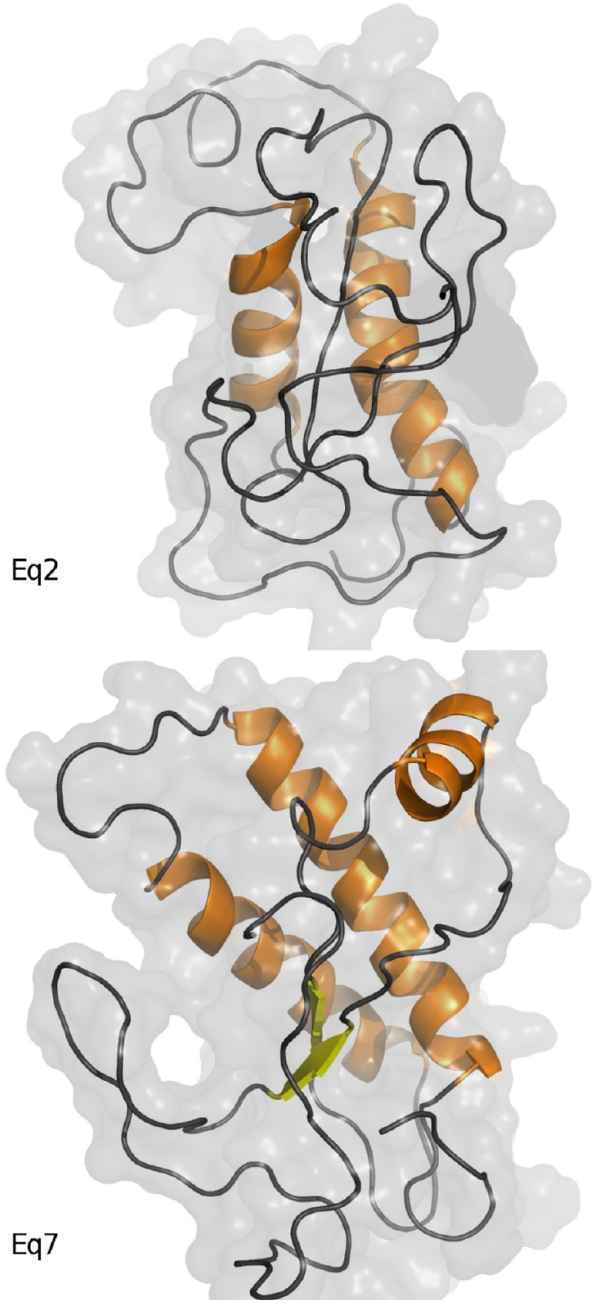

Figure 3. Central structures of the Eq2 and Eq7 simulations.

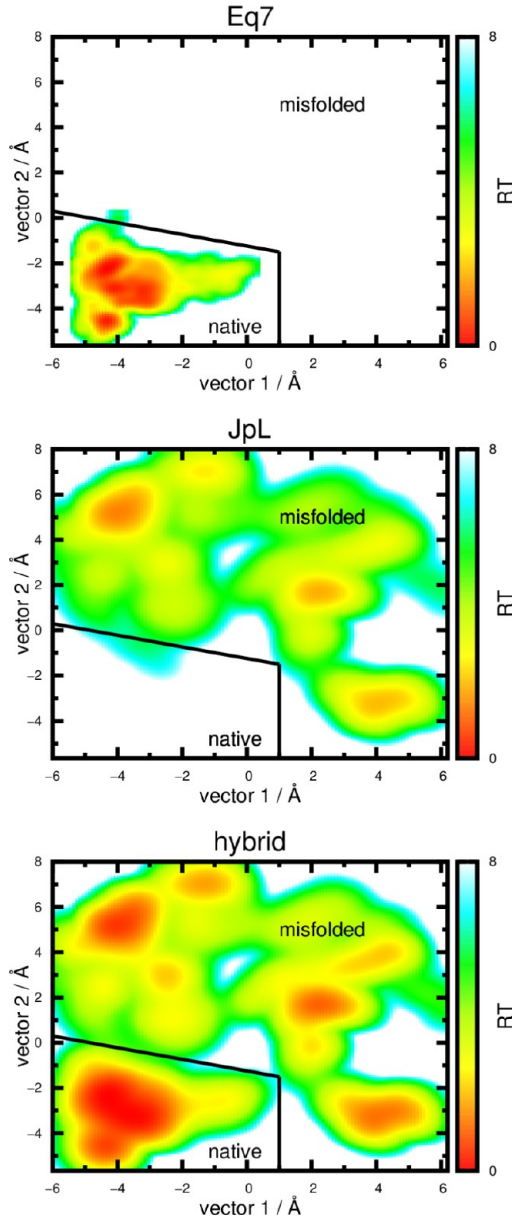

Figure 4. Energy landscapes at pH 7 using the first two PCs. The two first landscapes were obtained with the two groups of pH 7 simulations separately (the group of simulations used in each landscape is indicated). The third is a hybrid landscape of the first two. The native region is the one populated in the Eq7 simulations, and the misfolded region is the one populated in the JpL ones.

(Figure 3). In the central structure of the Eq7 simulations the global fold state of PrP is maintained, and the three helices remain almost the same size as in the original structure. On the other hand, in the central structure of the Eq2 simulations the HA is lost and the other two helices are shorter. Also, the global shape of the structure is significantly changed when comparing with the central structure of the Eq7 simulations.

In Figure 2a,c,e, the RMSD in relation to the central structures of pH 2 (black) and pH 7 (red) along time is depicted for three representative simulations. In addition, on the right side of each of these plots (Figure 2b,d,f) the RMSD values are plotted against each other, in order to evaluate if the sampled conformations were closer to those of pH 2 or 7. If the value is above (below) the $x = y$ line, the conformation is closer to the pH 2 (pH 7) central structure. Also, it is possible to use these plots to evaluate whether the protein is getting closer to pH 2 or pH 7 typical conformations, during the first 10 ns.

According to our RMSD calculations, in a significant number of the JpS simulations, the temporal curves present low fluctuations and the points are restricted to a small region in RMSD space (an example of this behavior is shown in Figure 2a,b). This observation suggests that the pH 7 had a stabilizing effect on the global protein structure, which is in agreement with the observations from previous work.[42]

In some cases, the simulation is moving away from both central structures (pH 2 and pH 7), as in Figure 2c,d. This observation is uncommon in the simulations started from early times in the misfolding pathway but becomes the most common scenario in the ones started from later times.

dx.doi.org/10.1021/jp3034837 | J. Phys. Chem. B 2012, 116, 8812−8821

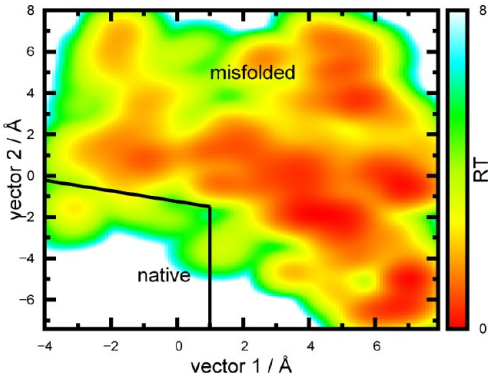

Figure 5. Energy landscape at pH 2 using the first two PCs. Native and misfolded regions are the same as in Figure 4.

In the simulations started from early times of the Eq2* simulation, there are a significant number of replicates in which the RMSD against the central structure of pH 7 decreases along the simulation time and the opposite happens with the RMSD against the pH 2 one (an example of this behavior is shown in Figure 2e,f). This observation suggests a partial reversibility event occurring in these simulations.

The RMSD results indicate that pH 7 can have a stabilizing effect on the protein structure, and this is very evident in the simulations started from conformations similar to the NMR structure. Moreover, at this point, it is possible to speculate that reversibility is indeed possible. However, it is more probable in simulations started at early times of the Eq2* simulation. This indicates that the most significant alterations in the misfolding transition might have occurred early in the Eq2* simulation.

The stabilizing effect of pH 7 in the PrP structure was already observed by several authors in both computational[34,37−39,42] and experimental studies.[30] Moreover, the reversibility of misfolding of PrP was also observed experimentally when pH is not too low.[30]

Conformational Analysis and Energy Landscapes. The PCA calculations were done with the equilibrated parts of 36 simulations (12 JpL, 12 Eq2, and 12 Eq7). The 2D space thus obtained was used to represent the simulation data. In spite of the first two PCs only accounting for 38% of the total variance, this 2D representation was enough to clearly discriminate between a misfolded and a native region.

With this methodology it is possible to obtain two energy landscapes at pH 7: one using the Eq7 and another one using JpL simulations (Figure 4). The first one is restricted to a relatively small region while the second has several basins scattered over the energy landscape. This indicates that the JpL simulations have more conformational variability than the simulations at pH 7 started from the native structure of PrP. This is not unexpected due to the large variety of starting conformations in JpL simulations. Furthermore, these two energy landscapes are only slightly overlapping which led us to distinguish two regions: native and misfolded, corresponding to Eq7 and JpL simulations, respectively.

Figure 4 also shows a hybrid landscape at pH 7 obtained by merging the Eq7 and JpL landscapes. In this energy landscape the relative depth of the native/misfolded regions might not be correct since we did not observe transitions between both regions. Nevertheless, this hybrid landscape should be a good overall representation of the conformational space of PrP at pH 7.

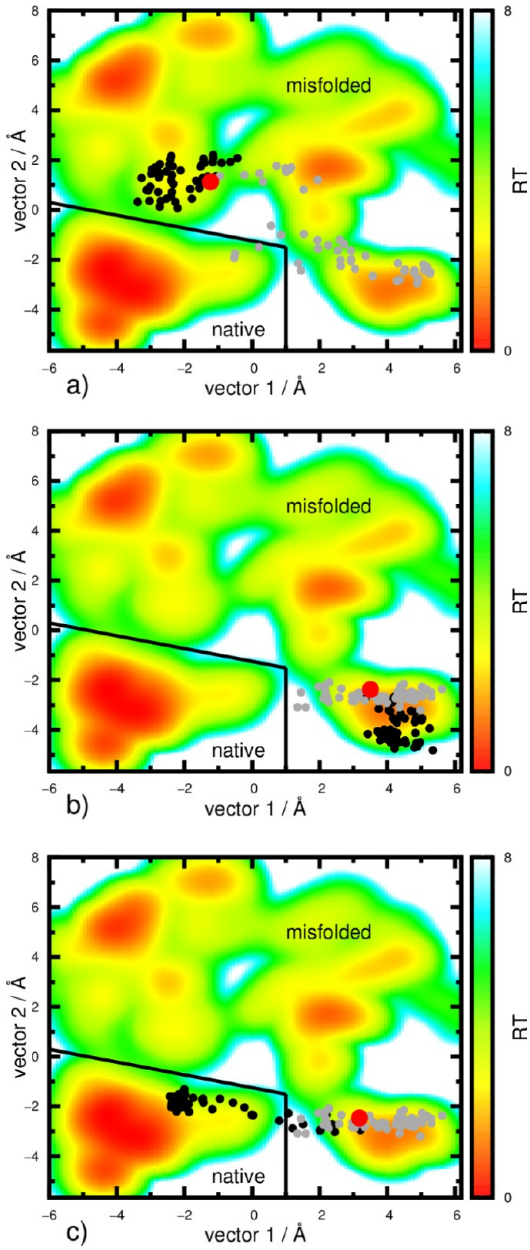

Figure 6. Hybrid energy landscape at pH 7 using the first two PCs and projections of the JpS simulations (black) and equivalent snapshots of the Eq2* simulation (gray). The starting points of the JpS simulations are also marked (red). Simulations 1.5a (a), 8.0b (b), and 8.0a (c). Snapshots are shown every 200 ps.

Using the described procedure, it was possible to obtain an energy landscape at pH 2 using the Eq2 simulations (Figure 5). Like for JpL, the landscape at pH 2 has many basins scattered over the energy landscape, which means that at this pH value the protein has a large conformational variability. However, the deeper basins change position after the change to pH 7, indicating the sampling of new regions previously unavailable at pH 2. As can be observed in Figure 5, the native region is barely populated at pH 2. The good discrimination between these two regions renders these landscapes a good tool to evaluate possible reversibility events in PrP misfolding.

The evolution of the short JpS simulations can now be followed on the hybrid landscape at pH 7 (Figure 4). Figure 6 and Figure S4 show this hybrid energy landscape together with

dx.doi.org/10.1021/jp3034837 | J. Phys. Chem. B 2012, 116, 8812−8821

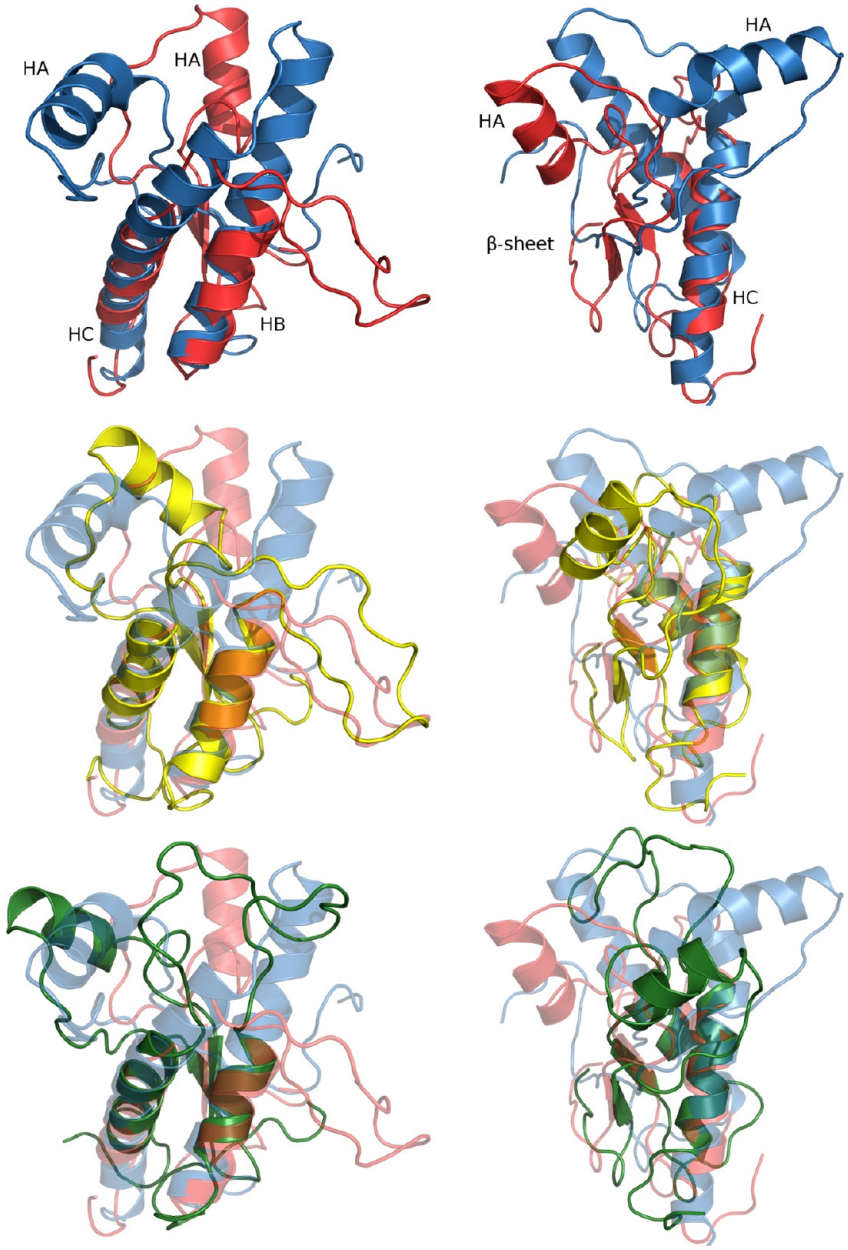

Figure 7. Conformational transition observed after changing to pH 7 in the 8.0a JpS simulation, showing starting snapshot (red), t = 3.0 ns snapshot (yellow), and final snapshot at t = 10.0 ns (green). The starting snapshot of the reference simulations Eq2* and Eq7* is also shown (blue). Residues of the HB and HC helices were fitted to the reference structure. Left panels: front view. Right panels: side view.

the projection of representative snapshots of the JpS simulations and the equivalent ones of the Eq2* simulation; this makes possible to compare the trajectories at pH 7 (black dots) and pH 2 (gray dots) when started from the same state (red dot). For example, Figure 6a corresponds to simulations started from the state t = 1.5 ns of Eq2*, showing 50 snapshots of the JpS simulation (every 200 ps from 0.0 to 10.0 ns) and the corresponding 50 snapshots of the Eq2* simulation (every 200 ps from 1.5 to 11.5 ns). In general, the simulations at pH 2 spread more over the landscape than the JpS simulations after the change in pH to 7, which reinforces the idea that pH 7 has a stabilizing effect. This is the most common scenario according to our PCA results. Figure 6a shows that, in the JpS simulation, the conformational space of the protein is confined to a small region of the landscape. Thus, while at pH 2 the conformation wanders away, after the change in pH the protein conformation is directed to a basin near the starting point. This observation is common in several replicates and is in agreement with the RMSD results (Figure 2a,b).

A less eventful scenario can be observed in Figure 6b. In this case, the JpS simulation does not move toward a basin. It moves in the landscape without an evident trend. However, it still samples slightly different regions compared to the Eq2* simulation, which is in agreement with our RMSD results (Figure 2c,d).

In several replicates the protein conformation leaves the misfolded region and moves toward the pH 7 deeper basin. Figure 6c shows the 8.0a simulation, where the most extensive reversibility transition occurred in our simulations. In this case, the protein starts in a typical misfolded region far from the deepest basin of pH 7, and it ends in the border of this basin, crossing a large distance on the landscape. This observation is

dx.doi.org/10.1021/jp3034837 | J. Phys. Chem. B 2012, 116, 8812−8821

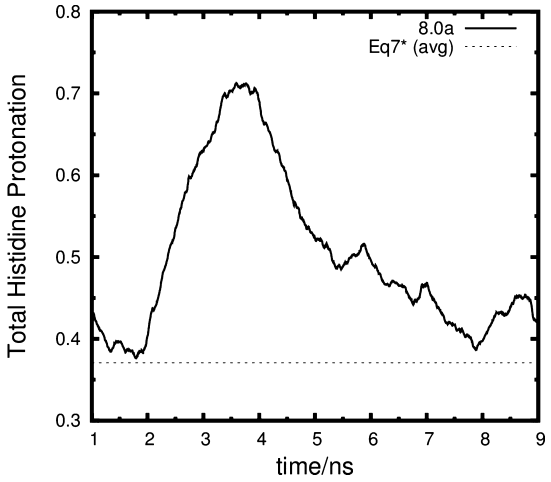

Figure 8. Total protonation of the histidines in a JpS simulation (8.0a). Data were averaged using a floating window with 2 ns size. The dashed horizontal line corresponds to the average value in the Eq7* simulation.

in excellent agreement with the rmsd results (Figure 2e,f). According to these analyses, it was possible to revert most of the effects of pH 2 in the PrP conformation accumulated over 8 ns of simulation. As previously mentioned, it was recently observed experimentally that PrP misfolding could be reverted unless very hash conditions (very low pH) were used.[30]

Although the PCA allowed us to obtain two separate regions in the hybrid landscape at pH 7 (native and misfolded), the lack of transitions between these two regions makes impossible to know their relative depths, and consequently, we are not able to infer on the nature of the stabilization of the folded state (thermodynamic versus kinetic).[8]

An Evident Reversibility Event. The results obtained for the simulation 8.0a led us to a detailed analysis of its conformational behavior. Figure 7 represents the starting, an intermediate and the final snapshots of this simulation, together with the common starting snapshot of the reference Eq2* and Eq7* simulations. There are two main regions in the protein that are changing in the direction of the reference structure (blue): (1) the loop between HB and HC is moving in the direction of the elongated arrangement of these two helices in the original structure, and (2) HA, maintaining its overall fold, is changing its position toward the reference conformation. Remarkably, these observations confirm that the pH change in this particular replicate originated, in 10 ns, an almost complete reversion of the three-dimensional effects caused by 8 ns of simulation at pH 2 (a short movie of this simulation is provided in movie S5 in the Supporting Information).

There are also other simulations where reversibility was observed to some extent, usually associated with the recovery of the HA position. A partial recovery of the relative position of HB and HC was also seen in several JpS simulations. Nevertheless, in the 8.0a JpS simulation the reversible transition is more evident and complete.

The movement of the loop between HB and HC was already observed in computational studies.[42] Also, the movement of HA is a common result in several computational studies.[40,42] In our study, we observed reversibility of these two significant pH-induced effects.

With the constant-pH MD methodology it is also possible to follow the titrating residues protonation states over time. Even though histidines prefer the two neutral tautomeric forms, we observed that all of them are actively (de)protonating and switching between tautomers. In simulation 8.0a, a strong peak in protonation appears between nanoseconds 2 and 5 (Figure 8), which corresponds to the major conformational transition (Figure 7 and video S5) where histidines were transiently more exposed to solvent. In many simulations, similar protonation peaks were observed, probably also due to histidine exposure to solvent but could not be unequivocally related to reversibility transitions.

CONCLUSIONS

In this work, we studied the reversibility of the misfolding of the prion protein by constant-pH molecular dynamics simulations.

The use of the DSSP criterion to evaluate reversibility events proved to be of limited use in the present study because of its dependence on the recovery of canonical secondary structure. This is very problematic due to the long time scales needed for such events to take place.[69]

The results from the RMSD and PCA energy landscapes showed that pH 7 had a large local stabilizing effect on the PrP conformations, which is in agreement with previous work.[30,34,37−39,42]

Reversibility events were observed when starting the pH 7 simulations from early altered conformations of the Eq2* simulation. This agrees with experimental results, suggesting that the misfolding transition is reversible when PrP is exposed to pH as low as 1.7.[30] Although simulation Eq2* originally started at the native basin, it departed from it and revisited its neighborhood very rarely during the simulation time (Figure 5); this might explain why no reversibility was observed at pH 7.0 when starting from later conformers of this simulation, which are probably too far from that basin to reach it within the simulated times.

Among the misfolded transitions that were promptly recovered with an increase of pH, we found an interesting long movement of helix HA, which has already been proposed to be a consequence of protonation,[42,40] and a movement of the loop between HB and HC, which aligns in the correct position for helix refolding.

This work confirmed the usefulness of the stochastic titration constant-pH MD method[44] when dealing with pH-induced conformational transitions. The present results bring new insights on the molecular details of the reversibility process already observed experimentally in the pH-induced misfolding of PrP .

ASSOCIATED CONTENT

Supporting Information

Two figures showing the starting snapshots for JpS and JpL simulations; one figure showing the RMSD plots for all JpS simulations and another showing the hybrid energy landscape at pH 7 and the projections of the JpS simulations; a movie of one of the JpS simulations where an evident reversibility event occurred. This material is available free of charge via the Internet at http://pubs.acs.org.

AUTHOR INFORMATION

Corresponding Author

*E-mail machuque@fc.ul.pt; Ph +351-21-7500112; Fax +351-21-7500088.

Notes

The authors declare no competing financial interest.

■ ACKNOWLEDGMENTS

We thank Maria José Calhorda, Paulo Jorge Costa, and João Henriques for fruitful discussions and Paulo J. Martel for a modified version of the g_rms tool of GROMACS. We acknowledge financial support from Fundação para a Ciência e Tecnologia, through projects PTDC/QUI-BIQ/105238/2008 and PEst-OE/QUI/UI0612/2011 and grant SFRH/BD/23506/2005.

■ REFERENCES

(1) Mouillet-Richard, S.; Ermonval, M.; Chebassier, C.; Laplanche, J. L.; Lehmann, S.; Launay, J. M.; Kellermann, O. *Science* **2000**, *289*, 1925−1928.
(2) Lehmann, S. *Curr. Opin. Chem. Biol.* **2002**, *6*, 187−192.
(3) Zahn, R.; Liu, A.; Lührs, T.; Riek, R.; von Schroetter, C.; García, F. L.; Billeter, M.; Calzolai, L.; Wider, G.; Wüthrich, K. *Proc. Natl. Acad. Sci. U. S. A.* **2000**, *97*, 145−150.
(4) Calzolai, L.; Zahn, R. *J. Biol. Chem.* **2003**, *278*, 35592−35596.
(5) Lee, S.; Antony, L.; Hartmann, R.; Knaus, K.; Surewicz, K.; Surewicz, W.; Yee, V. *EMBO J.* **2009**, *29*, 251−262.
(6) DeMarco, M. L.; Daggett, V. *C. R. Biol.* **2005**, *328*, 847−862.
(7) Chiesa, R.; Harris, D. A. *PLoS Biol.* **2009**, *7*, 439−443.
(8) Cohen, F. E.; Prusiner, S. B. *Annu. Rev. Biochem.* **1998**, *67*, 793−819.
(9) Prusiner, S. B. *Proc. Natl. Acad. Sci. U. S. A.* **1998**, *95*, 13363−13383.
(10) Collinge, J. *Annu. Rev. Neurosci.* **2001**, *24*, 519−550.
(11) Aguzzi, A.; Polymenidou, M. *Cell* **2004**, *116*, 313−327.
(12) Weissmann, C. *Cell* **2005**, *122*, 165−168.
(13) Abid, K.; Soto, C. *Cell. Mol. Life Sci.* **2006**, *63*, 2342−2351.
(14) Zou, W. Q.; Gambetti, P. *Cell. Mol. Life Sci.* **2007**, *64*, 3266−3270.
(15) Caughey, B.; Baron, G. S.; Chesebro, B.; Jeffrey, M. *Annu. Rev. Biochem.* **2009**, *78*, 177−204.
(16) Cobb, N. J.; Surewicz, W. K. *Biochemistry* **2009**, *48*, 2574−2585.
(17) Prusiner, S. B. *Science* **1982**, *216*, 136−144.
(18) Pan, K.-M.; Baldwin, M.; Nguyen, J.; Gasset, M.; Serban, A.; Groth, D.; Mehlhorn, I.; Huang, Z.; Fletterick, R. J.; Cohen, F. E. *Proc. Natl. Acad. Sci. U. S. A.* **1993**, *90*, 10962−10966.
(19) Shyng, S.-L.; Huber, M. T.; Harris, D. A. *J. Biol. Chem.* **1993**, *268*, 15922−15928.
(20) Magalhães, A. C.; Silva, J. A.; Lee, K. S.; Martins, V. R.; Prado, V. F.; Ferguson, S. S. G.; Gomez, M. V.; Brentani, R. R.; Prado, M. A. M. *J. Biol. Chem.* **2002**, *277*, 33311−33318.
(21) Arnold, J. E.; Tipler, C.; Laszlo, L.; Hope, J.; Landon, M.; Mayer, R. J. *J. Pathol.* **1995**, *176*, 403−411.
(22) Taraboulos, A.; Raeber, A. J.; Borchelt, D. R.; Serban, D.; Prusiner, S. B. *Mol. Biol. Cell* **1992**, *3*, 851−863.
(23) Borchelt, D. R.; Taraboulos, A.; Prusiner, S. B. *J. Biol. Chem.* **1992**, *267*, 16188−16199.
(24) Swietnicki, W.; Petersen, R.; Gambetti, P.; Surewicz, W. K. *J. Biol. Chem.* **1997**, *272*, 27517−27520.
(25) Jackson, G. S.; Hosszu, L. L. P.; Power, A.; Hill, A. F.; Kenney, J.; Saibil, H.; Craven, C. J.; Waltho, J. P.; Clarke, A. R.; Collinge, J. *Science* **1999**, *283*, 1935−1937.
(26) Hornemann, S.; Glockshuber, R. *Proc. Natl. Acad. Sci. U. S. A.* **1998**, *95*, 6010−6014.
(27) Gerber, R.; Tahiri-Alaoui, A.; Hore, P. J.; James, W. *Protein Sci.* **2008**, *17*, 537−544.
(28) Cobb, N. J.; Apetri, A. C.; Surewicz, W. K. *J. Biol. Chem.* **2008**, *283*, 34704−34711.
(29) Jenkins, D. C.; Pearson, D. S.; Harvey, A.; Sylvester, I. D.; Geeves, M. A.; Pinheiro, T. J. T. *Eur. Biophys. J.* **2009**, *38*, 625−635.
(30) Bjorndahl, T. C.; Zhou, G. P.; Liu, X.; Perez-Pineiro, R.; Semenchenko, V.; Saleem, F.; Acharya, S.; Bujold, A.; Sobsey, C. A.; Wishart, D. S. *Biochemistry* **2011**, *50*, 1162−1173.
(31) Chiti, F.; Dobson, C. M. *Annu. Rev. Biochem.* **2006**, *75*, 333−366.
(32) Shamsir, M. S.; Dalby, A. R. *Proteins* **2005**, *59*, 275−290.
(33) El-Bastawissy, E.; Knaggs, M. H.; Gilbert, I. H. *J. Mol. Graphics Modell.* **2001**, *20*, 145−154.
(34) Gu, W.; Wang, T.; Zhu, J.; Shi, Y.; Liu, H. *Biophys. Chem.* **2003**, *104*, 79−94.
(35) Chen, W.; van der Kamp, M.; Daggett, V. *Biochemistry* **2010**, *49*, 9874−9881.
(36) Barducci, A.; Chelli, R.; Procacci, P.; Schettino, V. *Biophys. J.* **2005**, *88*, 1334−1343.
(37) Alonso, D. O. V.; DeArmond, S. J.; Cohen, F. E.; Daggett, V. *Proc. Natl. Acad. Sci. U. S. A.* **2001**, *98*, 2985−2989.
(38) Langella, E.; Improta, R.; Barone, V. *Biophys. J.* **2004**, *87*, 3623−3632.
(39) DeMarco, M. L.; Daggett, V. *Biochemistry* **2007**, *46*, 3045−3054.
(40) van der Kamp, M.; Daggett, V. *Biophys. J.* **2010**, *99*, 2289−2298.
(41) Langella, E.; Improta, R.; Crescenzi, O.; Barone, V. *Proteins* **2006**, *64*, 167−177.
(42) Campos, S. R. R.; Machuqueiro, M.; Baptista, A. M. *J. Phys. Chem. B* **2010**, *114*, 12692−12700.
(43) Morrissey, M. P.; Shakhnovich, E. I. *Proc. Natl. Acad. Sci. U. S. A.* **1999**, *96*, 11293−11298.
(44) Baptista, A. M.; Teixeira, V. H.; Soares, C. M. *J. Chem. Phys.* **2002**, *117*, 4184−4200.
(45) Machuqueiro, M.; Baptista, A. M. *J. Phys. Chem. B* **2006**, *110*, 2927−2933.
(46) Machuqueiro, M.; Baptista, A. M. *Biophys. J.* **2007**, *92*, 1836−1845.
(47) Machuqueiro, M.; Baptista, A. M. *Proteins* **2008**, *72*, 289−298.
(48) Machuqueiro, M.; Baptista, A. M. *J. Am. Chem. Soc.* **2009**, *131*, 12586−12594.
(49) James, T. L.; Liu, H.; Ulyanov, N. B.; Farr-Jones, S.; Zhang, H.; Donnes, D. G.; Kaneko, K.; Groth, D.; Mehlhorn, I.; Prusiner, S. B.; Cohen, F. E. *Proc. Natl. Acad. Sci. U. S. A.* **1997**, *94*, 10086−10091.
(50) Campos, S. R. R.; Baptista, A. M. *J. Phys. Chem. B* **2009**, *113*, 15989−16001.
(51) Berendsen, H. J. C.; van der Spoel, D.; van Drunen, R. *Comput. Phys. Commun.* **1995**, *91*, 43−56.
(52) Lindahl, E.; Hess, B.; van der Spoel, D. *J. Mol. Model.* **2001**, *7*, 306−317.
(53) van der Spoel, D.; Lindahl, E.; Hess, B.; Groenhof, G.; Mark, A. E.; Berendsen, H. J. C. *J. Comput. Chem.* **2005**, *26*, 1701−1718.
(54) Oostenbrink, C.; Villa, A.; Mark, A. E.; van Gunsteren, W. F. *J. Comput. Chem.* **2004**, *25*, 1656−1676.
(55) Hermans, J.; Berendsen, H. J. C.; van Gunsteren, W. F.; Postma, J. P. M. A. *Biopolymers* **1984**, *23*, 1513−1518.
(56) Tironi, I. G.; Sperb, R.; Smith, P. E.; van Gunsteren, W. F. *J. Chem. Phys.* **1995**, *102*, 5451−5459.
(57) Smith, P.; van Gunsteren, W. *J. Chem. Phys.* **1994**, *100*, 3169−3174.
(58) Berendsen, H. J. C.; Postma, J. P. M.; van Gunsteren, W. F.; DiNola, A.; Haak, J. R. *J. Chem. Phys.* **1984**, *81*, 3684−3690.
(59) Hess, B.; Bekker, H.; Berendsen, H. J. C.; Fraaije, J. G. E. M. *J. Comput. Chem.* **1997**, *18*, 1463−1472.
(60) Teixeira, V. H.; Cunha, C. A.; Machuqueiro, M.; Oliveira, A. S. F.; Victor, B. L.; Soares, C. M.; Baptista, A. M. *J. Phys. Chem. B* **2005**, *109*, 14691−14706.
(61) Bashford, D.; Gerwert, K. *J. Mol. Biol.* **1992**, *224*, 473−486.
(62) Gilson, M. K.; Sharp, K. A.; Honig, B. H. *J. Comput. Chem.* **1987**, *9*, 327−335.
(63) Baptista, A. M.; Soares, C. M. *J. Phys. Chem. B* **2001**, *105*, 293−309.
(64) Baptista, A. M.; Martel, P. J.; Soares, C. M. *Biophys. J.* **1999**, *76*, 2978−2998.

(65) Metropolis, N.; Rosenbluth, A. W.; Rosenbluth, M. N.; Teller, A. H.; Teller, E. *J. Chem. Phys.* **1953**, *21*, 1087−1092.
(66) Jolliffe, I. T. *Principal Component Analysis*, 2nd ed.; Springer-Verlag: New York, 2002.
(67) Silverman, B. W. *Density Estimation for Statistics and Data Analysis*; Chapman and Hall: London, 1986.
(68) Kabsch, W.; Sander, C. *Biopolymers* **1983**, *22*, 2577−2637.
(69) Kubelka, J.; Hofrichter, J.; Eaton, W. *Curr. Opin. Struct. Biol.* **2004**, *14*, 76−88.